

Performance Characteristics of Hot-dip and Plasma Spray Aluminide Coated Nickel-Based Superalloy 718 under Cyclic Oxidation in Water Vapour

Pius Kibet KOECH*, Chaur Jeng WANG

Department of Mechanical Engineering, National Taiwan University of Science and Technology, No. 43 Keelung Road, Section 4, Taipei 10672, Taiwan, ROC

crossref <http://dx.doi.org/10.5755/j01.ms.25.4.21334>

Received 15 August 2018; accepted 12 October 2018

Aluminium coating due to its ability to form stable alumina oxide scale are commonly used to protect materials such as inconel 718 superalloys at high operational temperatures. Relevant properties of the oxide scale formed; growth rate and coating adherence is not only determined by the composition of the coating material used but is also influenced by the coating manufacturing process and the test condition. In the present work, effect of water vapour and thermocycling commonly prevailing on the morphology and composition of the alumina scales formed during high temperature oxidation was studied using hot-dip and plasma spray aluminium coatings. The coatings highly improved oxidation resistance of the alloy substrate with hot dip coating showing the lowest mass change compared to plasma spray. The results also show that the hot-dip coating has an inherently different morphology and growth rate compared to those formed on the plasma spray coating. High rate of oxidation, spallation and large voids with little protective alumina oxide layer were observed in moist condition test especially in plasma spray coatings.

Keywords: IN 718, hot-dip, plasma spray, aluminium coating, water vapour.

1. INTRODUCTION

Nickel based inconel (IN) 718 superalloy is widely used in aerospace, nuclear, chemical and tooling industry due to its excellent tensile strength, impact strength, creep resistance, oxidation and corrosion resistance at extremely high application temperatures [1–4]. Solid solution and precipitation hardening are two main mechanisms known for strengthening of nickel-based superalloys [5]. IN 718 is thus a precipitation strengthened nickel-based austenite superalloy where the particles γ' (Ni_3Al) and γ'' (Ni_3Nb) both precipitates simultaneously or sequentially above 550 °C, depending on the chemical compositions of Ti, Al and Nb [6, 7]. Common phenomenon reported is that γ' precipitates out first from γ - matrix, then γ'' phase nucleates heterogeneously at the γ'/γ interface and tends to merge with γ' particles creating a γ'/γ'' co-precipitates [8, 9]. When exposed to temperatures above 650 °C, the metastable γ'' particle transforms to the detrimental stable δ phase which precipitates at the grain boundaries. Studies shows that α -Cr also forms in addition to delta δ phase and is attributed to the depletion of Ni and an enrichment of Cr as a result of Cr rejection during delta δ phase formation. However high content of Cr leads to the reduction of creep strength. The δ - phase which is a major phase in such high temperatures is also attributed to loss of mechanical properties such as ductility, creep resistance and hardness [10–13].

IN 718 develops chromia protective oxide layer when exposed to high temperature oxidizing conditions. However, such protective oxide is susceptible to cracking and subsequent spallation leading to breakaway oxidation

especially under thermal cycling condition. With prolonged oxidation at high temperatures, aluminum is found to precipitate as an internal oxide beneath the chromium oxide scale. Other elements such as manganese which is found to be incorporated into the scale as MnCr_2O_4 is reported to improve oxide adherence as well as reducing chromium evaporation rate by lowering vapour pressure of CrO_3 [14]. Titanium just like aluminum has got high affinity of oxygen and thus have a strong tendency to form an oxide. Formations of NiCr_2O_4 and NiFe_2O_4 spinels are however reported to increase the Pilling-Bedworth ratio for Cr oxidation which contributes to lateral spallation of oxide scale [15].

The efforts to improve temperature stability of IN 718 has been going on with main focus on surface modification. Several surface modifications techniques are categorized as either surface treatments or surface coatings. Electro-polishing, heat treatment, shot peening, sandblasting, laser or chemical passivation are some of the surface treatments commonly carried out whose aim is to have energy stored on the surface region of the material in form of dislocations. Some of the surface coatings employed are cladding, sputtering, ion-implantation, pack cementation, micro-arc oxidation, thermal spray and hot-dip coating among others [16–19]. Surface coatings mainly thermal-spray and hot-dip coatings have recently found increasing use especially for high-temperature engineering applications due to their affordability and ease of use even in complex parts. Furthermore, they have added advantages such as time effectiveness, short processing time, flexibility among others. Aluminum is the consumable material commonly used for surface coatings during hot-dip or plasma spray due

* Corresponding author. Tel.: +886-963-544-340;
E-mail address: d10303809@mail.ntust.edu.tw (P.K. Koech)

to its ability to form a stable alumina oxide scale [15, 20]. This article therefore is aimed to study the performance of hot-dip and plasma spray aluminium coatings under cyclic oxidation in dry and in moist vapour condition.

2. EXPERIMENTAL DETAILS

2.1. Sample preparation

Nickel based IN 718 superalloy specimens of chemical composition shown in Table 1 were sectioned to rectangular sizes of 15 mm × 15 mm × 2 mm using water-cooled abrasive cut-off wheel. Specimens were mechanically ground to 800 grit SiC papers then holes of about 1.5 mm in diameter were drilled for suspension during hot-dip coating.

Table 1. Chemical composition of Inconel 718 used in this research

Element	Ni	Cr	Fe	Ti	Si	Al	Nb	Mo
wt.%	Bal.	18.46	17.82	1.07	0.38	0.46	5.52	2.83
at.%	Bal.	20.58	18.66	0.82	0.46	0.71	3.65	1.73

2.2. Specimen coating

All abraded and polished specimens were degreased ultrasonically in acetone for five minutes, then cleaned in a solution of 10 wt.% NaOH and 15 vol.% H₃PO₄ for 15 seconds and finally rinsed in fresh water, ethanol and dried. After cleaning, flux coated specimens were immersed into a molten bath of pure aluminum (99.5 wt.% Al) maintained at 700 °C for only one minute. Immersion and removal speed from molten bath was 15 cm/min. Aluminized hot-dipped specimens were then cleaned to remove oxide flux attached to the surface using solution of nitric, phosphoric acid and water in a 1:1:1 volume ratio at 25 °C, then finally rinsed in fresh water, ethanol and dried. Commercially pure aluminum (99.5 wt.% Al) was used as a spray consumable to create a coating on sand blasted and ultrasonically cleaned surfaces of IN 718 specimens for plasma spray coatings. Gas flow rate of 4.2 m³/h at 5500 °C with particle velocity of 240 m/s and spray rate of 2.5 kg/h were used.

2.3. Oxidation test

Bare and aluminium coated IN 718 specimens were cyclically oxidized inside a horizontal tube furnace at 650 and 750 °C in both dry air and moist air by passing dry carrier gas to the hot chamber zone at a flow rate of 200 cc/min maintained at 1 atm. For cyclic oxidation under water vapour condition, moist air was supplied to oxidation zone by passing dry carrier gas through hot water bath kept at 76 °C with vapour pressure of about 0.397 atm. The specimen exposure time was 10 hours in hot chamber and 30 minutes in room temperature a cycle for up to 90 hours (9 cycles) in hot chamber. Specimens were picked after each cycle for average mass change measurements using precision electron balance (Mettler Toledo) with an accuracy of 0.1 mg so as to assess high-temperature performance of the aluminium coatings on IN 718 alloy.

2.4. Cross-sectional and surface morphology characterization

Characterization of the surface morphology and cross-sectional microstructure were carried out using JEOL JSM-

6390 scanning electron microscopy (SEM), while the distributions of elements in various solid phases were analyzed using an energy dispersive X-ray spectroscopy (EDS) and electron probe microanalysis (EPMA). Phase analysis of oxidation scales and corrosion products on surfaces of the bare and aluminized coated specimens were conducted using Bruker D2-Phaser X-ray diffraction (XRD) machine with a range of 20° ≤ 2θ ≤ 80° diffraction angle at steps of 0.02/step. Diffraction patterns from XRD data were analyzed using DIFFRAC.EVA software.

3. RESULTS

3.1. As-deposited aluminium coating specimens

Cross-sectional micrograph, surface morphology and XRD patterns of as coated aluminized hot-dip and plasma spray alloy specimens are given in Fig. 1.

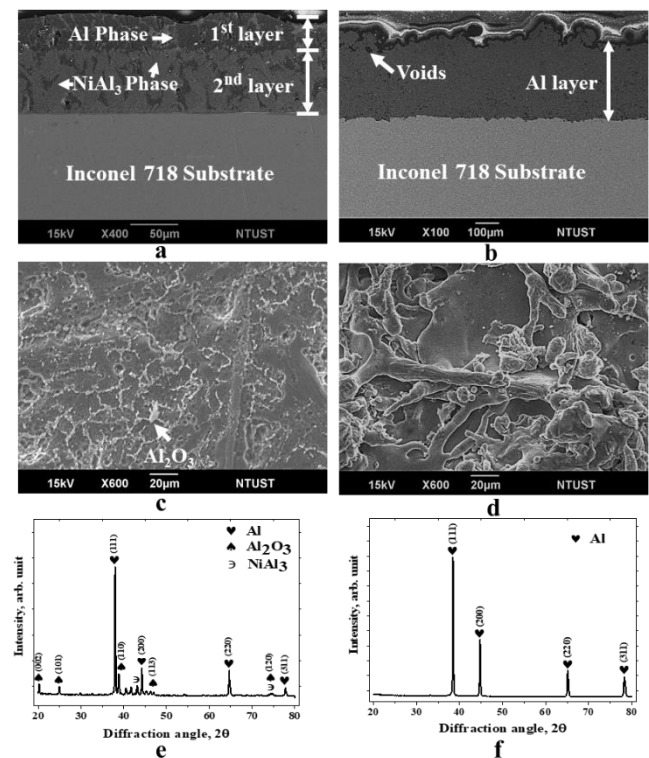


Fig. 1. Cross-sectional micrograph, SEM surface morphology and XRD pattern of as coated aluminized alloy IN 718: a, c, e – hot-dip; b, d, f – plasma spray specimens respectively

The coating on the hot-dip specimen adhered firmly to the IN 718 substrate with no signs of cracks, porosities or delamination as seen in the cross-sectional micrograph of Fig. 1 a. The 1st layer on top of the coating comprise of a dark-grey compact aluminum phase with a thickness of approximately 30 μm. The 2nd layer consists of light-grey NiAl₃ phase with a thickness of about 60 μm formed at the interface between the substrate and the aluminum layer. The amount and depth of the inter-diffusion phases formed were determined by the hot-dip duration, the activity of molten aluminum on the outer zone of the coating and the activities of nickel among other minor elements on the substrate side. The cross-sectional micrograph for plasma spray coating in Fig. 1 b shows that only one layer of aluminum coating formed on top of the substrate. The aluminum coating layer

formed consists of deposited splats with presence of some Al_2O_3 oxides and voids ingrained at the grain boundaries of the deposited splats. Surface morphology of as-coated hot-dip specimen consists of aluminium grains as in Fig. 1 c. The grains contain oxides of Al_2O_3 on the ridges while the crater region and entire surface is mainly made of aluminum layer with presence of some intermetallic phases of NiAl_3 as determined by EDS analysis. The X-ray diffraction (XRD) analysis of as-coated hot-dip specimen depicted in Fig. 1 e also indicates that the surface structure consists mainly of aluminum layer with some peaks of Al_2O_3 and NiAl_3 .

The surface morphology for plasma spray coating shown in Fig. 1 d consists of irregular grain boundaries with existence of some voids and pores. Both EDS analysis and XRD pattern results given in Fig. 1 f indicates that surface morphology of plasma spray coating consists mainly of aluminum layer.

3.2. Kinetics of oxidation

The kinetics of cyclic oxidation curves for bare IN 718 superalloy and aluminized coatings done in dry and moist air at 650°C and 750°C respectively are given in Fig. 2. The mass changes during thermal cycling of all tested specimens both in dry and moist air indicates that the rate of oxidation increased with both the duration and exposure temperature. The mass gain for uncoated specimens in dry air exhibited highest rate of oxidation. The mass changes in all conditions and temperatures are higher during the early stages of oxidation but changes to steady state with increased exposure time. During early stages of oxidation, rapid formation and growth of protective oxide scale inhibits inward diffusion of oxygen and outward diffusion of alloy ions. It is also evident that both the hot-dip and plasma-sprayed coatings improved oxidation resistance of the alloy. In terms of mass changes, no significant difference in performance of the two different aluminum coatings namely hot-dip and plasma-spray was observed compared to bare substrate. However, hot-dip coatings with the lowest mass change demonstrated that it is slightly much better than plasma-sprayed coatings in improving the oxidation resistance of the alloy. Oxidation rate for both aluminum coatings are slightly higher in moist vapor condition both at 650°C and 750°C . The mass change curves in moist vapour also shows undulated nature after about 40 to 50 hrs which suggests that spallation of oxide scale and re-oxidation took place. Both the bare and coated specimens in all conditions follow a parabolic rate law. The difference between the bare alloy and aluminum coated specimens could be attributed to the ability of the later to re-heal after oxide spallation due formation of a protective alumina scale.

3.3. Surface morphology and cross-sectional micrograph of hot-dip coatings

Surface morphology of the oxide scale formed on aluminized hot-dip specimens at 650°C and 750°C are given in Fig. 3. The EDS analysis infer that the surface of the coating consists mainly of Al_2O_3 oxide after 90 hrs in dry air at 650°C for Fig. 3 a. Specimens oxidized in dry air at 750°C indicates some scale spallation after 10 hrs as shown in Fig. 3 b. The surface comprises of Al_2O_3 scale while the area under spallation is an exposed aluminum layer.

Analysis of such spalled portion does not show any evidence of oxide reformation during the 10 hrs isothermal oxidation an indication that spallation took place during cooling of the specimen. Scale spallation, oxide-reformation and regrowth of aluminum-oxide nodules increased with cyclic oxidation shown in Fig. 3 c after 90 hrs at 750°C . Besides spallation and oxide reformation, EDS analysis confirms presence of $\text{Al}_{1.98}\text{Cr}_{0.02}\text{O}_3$ in addition to Al_2O_3 oxides indicating outward diffusion of chromium and other substrate elements with increased exposure time and temperature. Other phases detected in small amounts are NiAl_3 , Ni_2Al_3 with oxides of NiO and NiAl_2O_4 .

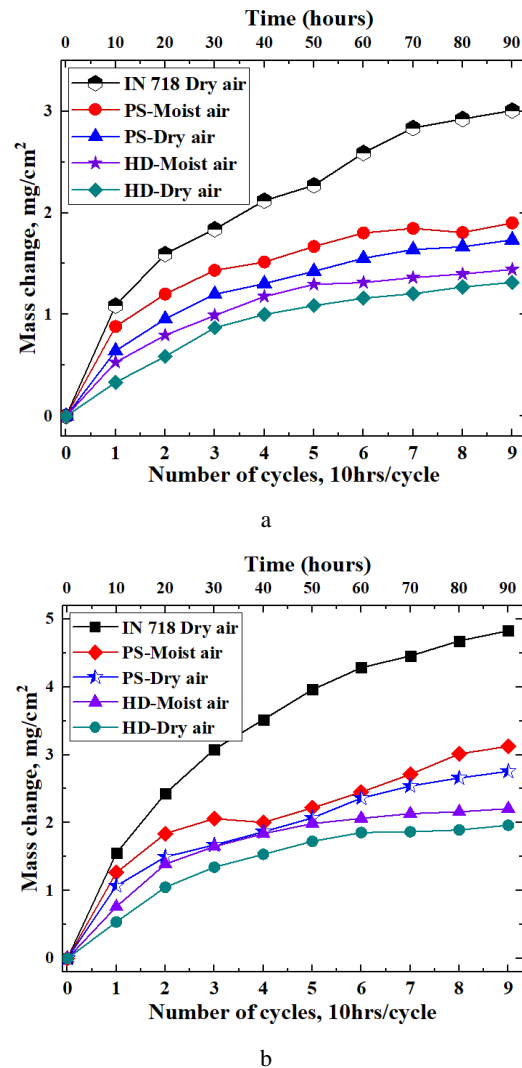


Fig. 2. Mass changes of bare IN 718, hot-dip and plasma spray coated specimens during 90 hrs cyclic oxidation in dry and moist air at: a– 650°C ; b– 750°C

Oxide spallation and existence of some cracks were observed after 90 hrs for specimens oxidized in moist air at 650°C as shown in Fig. 3 d. The oxide scale composed mainly Al_2O_3 with minor elements of nickel indicating presence of NiAl_3 phases. However, hot-dip specimens exposed to high-temperature at 750°C after 10 hrs in moist air experienced high spallation and surface cracking as shown in Fig. 3 e. EDS analysis did not show any signs of scale reformations on the debonded sections indicating that scale spallation took place only during specimen cooling and not during isothermal high-temperature exposure.

Oxide scale spallation and voids increased with cyclic oxidation in moist condition after 90 hrs at 750 °C as shown in Fig. 3 f. Oxide reformation seems to reduce in moist air compared to those in dry condition. Porous plate-like spinel of NiAl_2O_4 was also detected on the surface as shown in the enlarged portion of Fig. 3 f. Other minor oxides detected were $\text{Al}_{1.98}\text{Cr}_{0.02}\text{O}_3$, Fe_2O_3 , NiO , NiFe_2O_4 and FeCr_2O_4 .

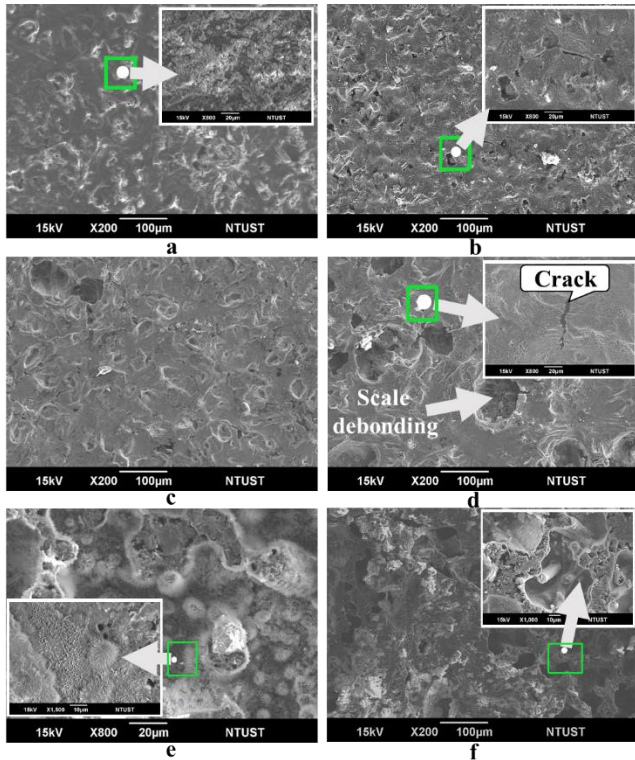


Fig. 3. SEM surface morphology of hot-dip specimens oxidized in dry air at: a–650 °C for 90 hrs; b–750 °C for 10 hrs; c–750 °C for 90 hrs, and in moist air at: d–650 °C for 90 hrs; e–750 °C for 10 hrs; f–750 °C for 90 hrs

Cross-sectional micrographs of hot-dip aluminumized IN 718 specimens after high-temperature exposure in dry and moist air are given in Fig. 4. Aluminium coating layer transformed into various distinct layers. A thin layer of Al_2O_3 oxide scale formed on the surface of the aluminide coating while an aluminum layer formed beneath it after 90 hrs in dry air at 650 °C as shown in Fig. 4 a. A layer comprising of NiAl_3 phase formed in the middle while Ni_2Al_3 is next to the substrate. The coating layers does not show any signs of porosities or delamination. However, specimens exposed to high-temperature at 750 °C after 10 hrs in dry air given in Fig. 4 b indicates formations of voids within the aluminum layer. A thin layer of Ni_2Al_3 is seen to have formed at the interface between the substrate and the NiAl_3 phase as determined by EDS analysis. With increased oxidation time, voids are seen to extend to NiAl_3 layer after 90 hrs in dry air at 750 °C as shown in Fig. 4 c. The Ni_2Al_3 layer increased with cyclic oxidation and temperature while the aluminum layer and NiAl_3 gets depleted with increased voids. Depletion of aluminum could be attributed to inward diffusion to enhance formation of NiAl intermetallic layers and outward diffusion for the reformation of aluminum oxide layer. Fig. 4 d for hot-dip specimen oxidized in moist air at 650 °C after 90 hrs unlike in dry air shows presence of voids highly dispersed within

the aluminum layer with fragmented and reduced thickness of Al_2O_3 scale. Thickness of Ni_2Al_3 intermetallic layer and number of voids observed in Fig. 4 e after 10 hrs and Fig. 4 f after 90 hrs increased with exposure time while the aluminum layer gets depleted for specimens exposed to moist air at 750 °C. Cracks are also seen to form at the interface of Al layer and the NiAl_3 phase after 90 hrs as observed in Fig. 4 f. The elemental compositions of Al, Ni, Cr and Fe along the Y-Y axis of Fig. 4 d and f is given in Fig. 5 a and b respectively. The inward diffusion of Al and outward diffusion of Ni, Cr and Fe among other elements contributes to the growth of such observed NiAl intermetallic layers.

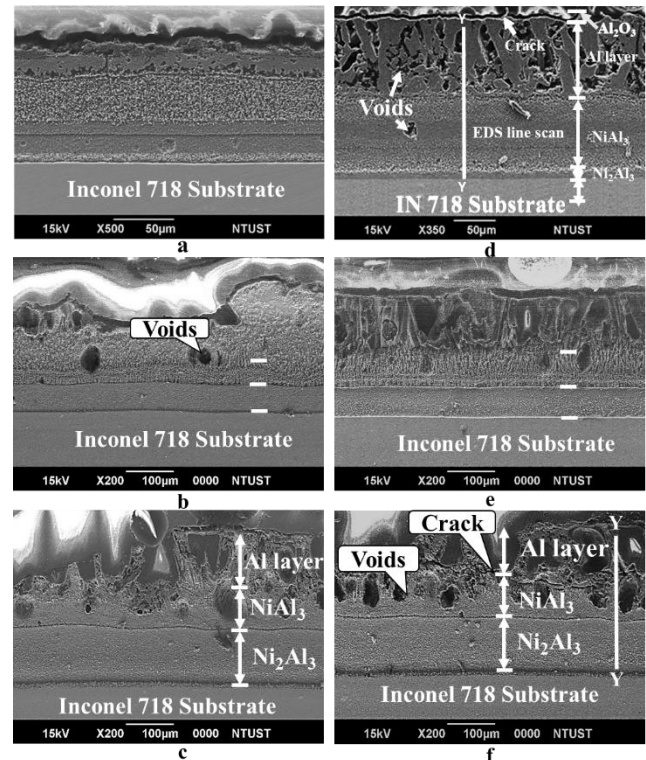


Fig. 4. Cross-sectional micrographs of hot-dipped specimens oxidized in dry air at: a–650 °C for 90 hrs; b–750 °C for 10 hrs; c–750 °C for 90 hrs, and in moist air at d–650 °C for 90 hrs; e–750 °C for 10 hrs; f–750 °C for 90–hrs

3.4. Effect of plasma spray coatings on the high temperature cyclic oxidation

Fig. 6 shows the surface morphology that developed on the plasma spray coated IN 718 alloy specimens after various durations of cyclic oxidation in dry and moist air at 650 and 750 °C. Unlike in hot-dip coating specimens given in Fig. 3, surface morphology of plasma spray has got irregular grain shapes with grooves along the splat boundaries. The oxide scale consists of Al_2O_3 with porosity's along the lower portion of the ridges as shown in Fig. 6 a after 90 hrs in dry air at 650 °C. Cracks and aluminum depletion on the surface seems to increase with exposure time as observed in Fig. 6 b after 10 hrs compared to Fig. 6 c after 90 hrs in dry air at 750 °C. EDS analysis indicates that besides Al_2O_3 , other elements such as Ni, Cr and Fe were detected on the surface due to outward diffusion of substrate elements towards the surface of the coating. At points indicated by letters 'A', 'B' and 'C' in

Fig. 6 c, oxides of Al_2O_3 , NiO and spinels of NiAl_2O_4 formed on the surface after 90 hrs. Corresponding chemical compositions of the points indicated are given in Table 2.

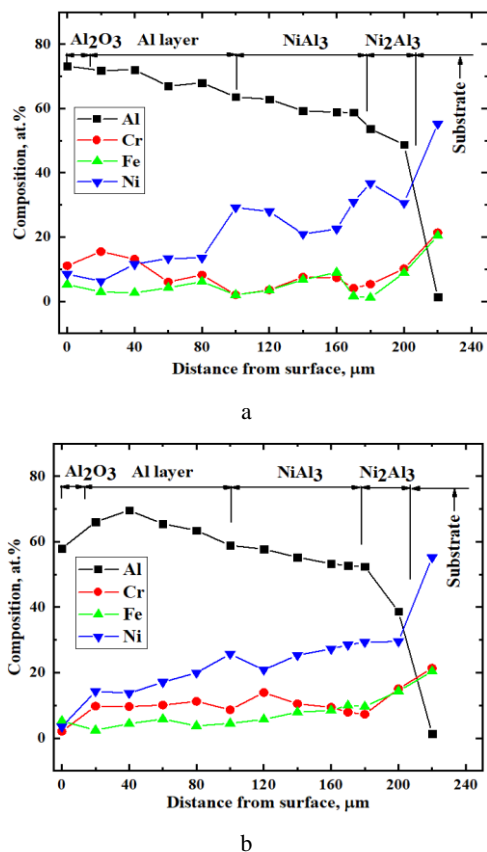


Fig. 5. EDS results for elemental compositions Al, Cr, Fe and Ni across the coating layer axis (Y-Y) after 90 hrs in moist air for: a – Fig. 4 d at 650 °C; b – Fig. 4 f at 750 °C

Surface morphology of specimens oxidized in moist air for 90 hrs at 650 °C given in Fig. 6 d, after 10 hrs at 750 °C shown in Fig. 6 e and after 90 hrs at 750 °C in Fig. 6 f shows raised oxide nodular of Al_2O_3 with deep furrows and ridges appearing along the splat boundaries. Furrows and cracks are seen to be more profound compared to those in dry air and increases with exposure time indicating that splat boundaries are more susceptible to moist oxidation attack. Water vapour trapped at the furrows weakens the bonding at the splat boundaries inducing more cracks as shown. Increased cracks and furrows facilitates high rate of oxidation due to increased surface area. The surface of the coating at the point indicated by letter ‘D’ in Fig. 6 f, consists of Al_2O_3 oxide while at the furrow like portion indicated by letter ‘E’ shows that besides Al_2O_3 , minor oxides of $\text{Al}_{1.98}\text{Cr}_{0.02}\text{O}_4$, NiO or NiAl_2O_4 spinels could have formed. Chemical compositions indicated at points ‘D’ and ‘E’ are given in Table 2.

Table 2. Chemical composition (at.%) of points indicated in Fig. 6 by EDS analysis

Position	Al	Cr	Ni	Fe	O
A	55.32	–	8.29	–	36.39
B	53.98	–	18.62	–	27.41
C	53.12	–	15.95	–	30.93
D	50.01	–	–	–	49.99
E	54.89	2.86	9.96	1.99	30.29

Cross-sectional micrographs of aluminized plasma spray coated specimens exposed to high temperature oxidation in dry and moist air at various durations are given in Fig. 7. After 90 hrs in dry air at 650 °C shown in Fig. 7 a, voids are observed at the Al coating layer with micro cracks between Al_2O_3 oxide layer and the aluminum coating. However, in moist air as in Fig. 7 d, aluminum layer is separated from the NiAl_3 intermetallic layer by a crack with diminished oxide layer. For specimens oxidized at 750 °C, thin and compact layers of NiAl - intermetallics had formed after 10 hrs in dry air with some voids observed within the aluminum layer as observed in Fig. 7(b). However, in moist air after 10 hrs shown in Fig. 7(e), the voids have extended to the NiAl_3 intermetallic layer with high flaking of the oxide scale.

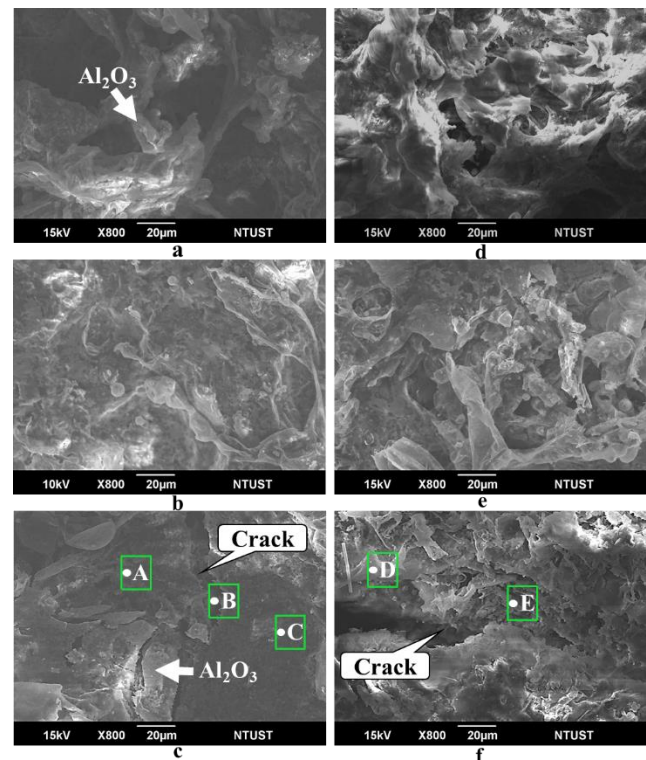


Fig. 6. SEM surface morphology of plasma spray specimens oxidized in dry air at: a – 650 °C for 90 hrs; b – 750 °C for 10 hrs; c – 750 °C for 90 hrs, and in moist air at: d – 650 °C for 90 hrs; e – 750 °C for 10 hrs; f – 750 °C for 90 hrs

The plasma spray coating could not withstand exposure to high-temperature for a prolonged period of time. There is an increased oxidation along the grain boundaries of the deposited splats with layer-shaped flaking of grains within the interface of oxide scale and aluminum layer after 90 hrs at 750 °C both in dry air, Fig. 7 c, and in moist condition as in Fig. 7 f. Voids within the coating layer are also seen to increase both in size and number with cyclic exposure time and a little more in specimens under cyclic oxidation in moist conditions. In Fig. 3 through Fig. 6, although no signs of coating delamination were observed, degradation of the aluminum coating is much high in plasma spray coatings compared to hot-dip coatings. EDS analysis for elemental compositions taken along the Y-Y axis of Fig. 7 d and f indicates that Cr, Fe and Ni diffused outwards from the substrate to the surface of the coating as shown in Fig. 8 a and b respectively.

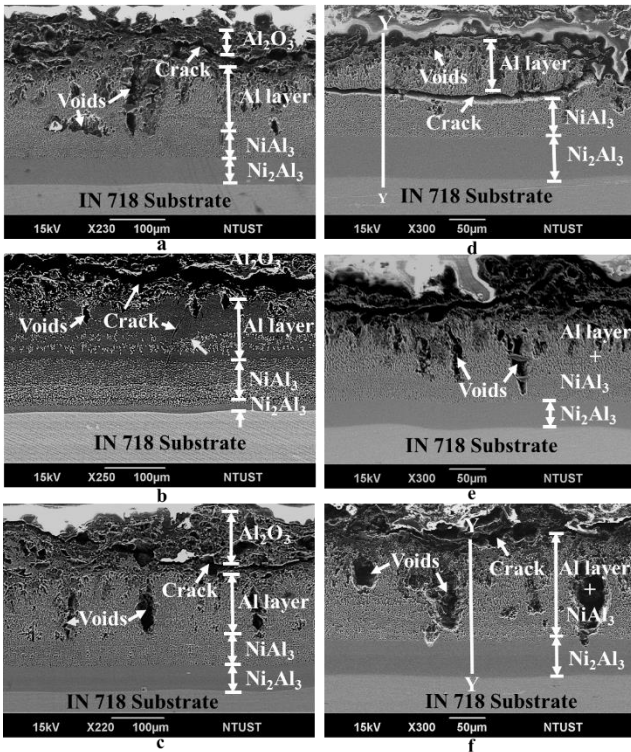


Fig. 7. Cross-sectional micrographs of plasma spray specimens oxidized in dry air at: a–650 °C for 90 hrs; b–750 °C for 10 hrs; c–750 °C for 90 hrs, and in moist air at: d–650 °C for 90 hrs; e–750 °C for 10 hrs; f–750 °C for 90 hrs

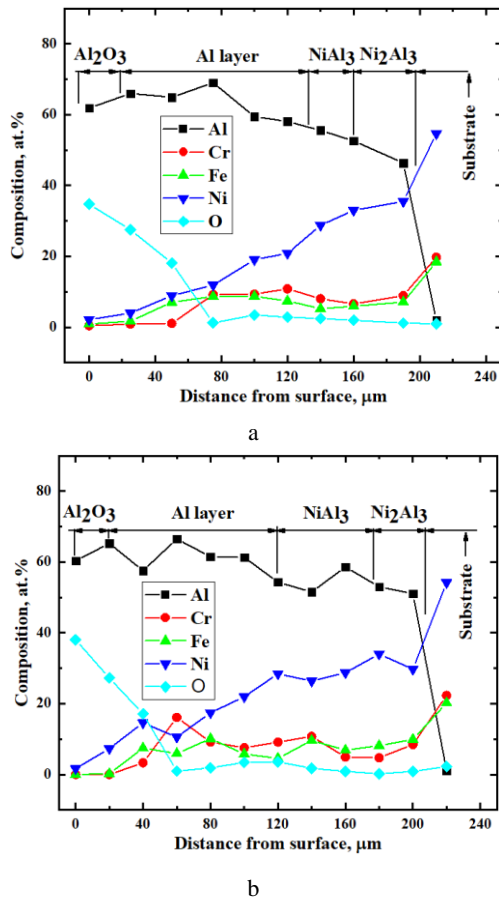


Fig. 8. EDS results for elemental compositions Al, Cr, Fe, Ni and O across the coating layer axis (Y-Y) after 90 hrs in moist air for: a–Fig. 7 d at 650 °C; b–Fig. 7 f at 750 °C

4. DISCUSSION

4.1. Formation mechanism of the coating layer on IN 718 specimens

According to experimental results, the as-deposited aluminized coatings consists of two layers in hot-dip and only one layer in plasma spray specimens shown in Fig. 1. The 1st layer in hot-dip specimens shown in Fig. 1 a is composed of aluminum phase and contains some dissolved nickel elements that were derived from the substrate. The 2nd layer consists of NiAl₃ - intermetallic phase formed beneath the aluminum layer. The formation mechanisms of the NiAl₃ among other intermetallic phases within the coating layer can be discussed based on the knowledge of the binary phase formation for a given elements [5, 21]. An interface between liquid and solid exists during hot-dip process in which the aluminum is in molten state as liquid while nickel among other elements in the substrate are in solid state. As the coating process takes place, the Ni, Cr and Fe from the IN 718 substrate dissolves and diffuses into the molten Al until the saturation level is reached then the extra atoms of elements such as Ni reacts with Al atoms to form intermetallic phase of NiAl₃. The NiAl₃ phase will then nucleate and grow in the supersaturated molten solution of Al near the interface forming a mixture of NiAl₃ phase and Al solution. With continuous advancement of substrate elements mainly Ni among other minor elements into the molten aluminum solution, the growth of NiAl₃ increases and continues to precipitates with increased hot-dip time. As the coated specimen is withdrawn from the aluminum molten solution allowing cooling and solidification to take place, the solubility of the substrate elements such as Ni in the Al solution is drastically reduced. The precipitation eventually takes place with the formation of a thin layer of NiAl₃ phase at the interface as observed in Fig. 1 a. The formation of NiAl₃ phase in the as-coated hot-dip specimens and absence of other phases such as Ni₂Al₃ attributes to complete consumption of Ni within the Al liquid solution. Thus, due to high surplus of Al, only intermetallic compound of Ni-Al with higher Al content such as NiAl₃ will form as seen in Fig. 1 [22]. Upon withdrawal from the molten bath, liquid aluminium due to surface tension effect solidifies to form a coating layer comprising of aluminum layer. Aluminum will also readily form oxides of Al₂O₃ upon withdrawal from molten metal due to its low free energy of oxide formation, thus the existence of alumina oxide [23].

The plasma spray as-coated specimen in Fig. 1 b consists of a single aluminum coating layer with existence of voids and pores. During plasma spray coating process, the atomized aluminum particles are oxidized forming entrapped oxides. With subsequent spray layer, existence of such oxides inhibits complete fusion of new aluminum splats to the already deposited one hence giving rise to presence of voids. Unlike hot-dip coating process where interdiffusion of elements takes place at the interface of coating and substrate, plasma spray coating which employ heat and velocity is characterized by near-zero dilution of the substrate due to mechanical bonding. Also, the substrate coated by plasma spray does not undergo any distortion,

interdiffusion or metallurgical degradation compared with hot-dip coatings due to its low deposition temperatures.

4.2. Effect of aluminum coatings on oxidation mechanism of IN 718 alloy

Aluminium coatings showed the lowest oxidation rate in Fig. 2 after 90 hrs cyclic oxidation as compared to bare substrate. Reduction in such mass change could be attributed to the formation of a more stable alumina oxide and intermetallic layer of NiAl_3 as shown in Fig. 3 through Fig. 7 and illustrated in Fig. 9 a, which are reported to offer improved oxidation resistance. However, coatings oxidized in moist air slightly has a higher mass change. This could be likely as a result of the crack formation either on the surface scale or within the aluminium layer which allowed access of H_2O to penetrate through paths of such cracks or voids. Reaction of H_2O and aluminum forms an alumina oxide with increased mass gain [24, 25]. Nevertheless, the plasma spray coatings have slightly high mass gain than the hot-dip coating. Surface morphology of aluminized plasma spray coatings in Fig. 6 has irregular grain shapes with grooves, voids and cracks along the splat boundaries which increases the surface area for oxidation to take place, giving rise to high mass gain as observed. Such irregular grains also trap water vapour acting as oxidation sites. Illustration for initial oxidation of plasma spray coatings is given in Fig. 9 d.

A continuous oxide layer of Al_2O_3 formed above a compact intermetallic and aluminum layers at 650 °C in dry air condition as given in Fig. 3 a for surface morphology and cross-sectional micrograph in Fig. 4 a. With increase in temperature, as in Fig. 3 b, c and Fig. 4 b, c at 750 °C, protective nature of aluminum coating is reduced due to increased number of voids. The surface morphology depicted in Fig. 3 d, e has Al_2O_3 oxide scale debonding with existence of some cracks. Oxides such as Al_2O_3 are highly brittle and the cracks existing on the surface of the coated specimens are attributed to residual stress on such brittle oxides during rapid cooling [26]. When the aluminum alloy is used as a protective coating on IN 718, the intermetallic layer NiAl_3 is not only consumed during interdiffusion for the growth of a brittle and less oxidation resistance phase such as Ni_2Al_3 but also for oxidation of itself. Oxidation of NiAl_3 gives rise to oxides of Al_2O_3 , NiO and spinels of NiAl_2O_4 as identified to exist in Fig. 3 through Fig. 6 with an illustration in Fig. 9 b, c. However, in moist condition as shown in Fig. 4 d, dissociation of water vapour into OH^- and H^+ which in turn are incorporated into oxide lattice with formation of weak Al-OH^+ bonds results to voids growth. Vacancy condensation due to fast outward diffusion of aluminum ions through the scale is reported to be the main reason for void formation in the oxide scale [23]. Such dissociation and void formation increases with temperature and oxidation duration as observed in Fig. 4. The dissociation of water vapour is also ascribed to weakening of the scale–alloy interfacial toughness thus promoting the formation of interfacial voids which accelerates spallation of the oxide scale with subsequent cracking of the coating [27, 28]. Results of hot-dip coating in Fig. 4 indicates that the Ni–Al intermetallic layers formed in the aluminum coating due to outward diffusion of nickel and not by inward diffusion of aluminum into the substrate. Such phenomenon

is evidenced by EDS elemental line profile given in Fig. 5 indicating steady outward diffusion of substrate elements Ni, Cr and Fe towards aluminum coating. The previous studies on oxidation of nickel-based superalloys with aluminium coatings also reported similar observation [5, 20, 29]. Conversely, degradation of the aluminum layer is due to inward diffusion of Al towards the substrate for the growth of Ni–Al intermetallic layers and outward for growth of Al_2O_3 . Depletion of such Al – contents are attributed to presence of Kirkendall voids in the coatings as illustrated in Fig. 9 b. Such voids in addition to presence of cracks within the coating layer acts as transport mechanism channel for oxidation of NiO and subsequent transformation into NiAl_2O_4 spinel as detected by EDS analysis [30]. The porous nature of NiAl_2O_4 spinel could further act as sites for internal oxidation and degradation of the aluminum layer as observed in Fig. 3 f with illustration in Fig. 9 c. Spinel of NiAl_2O_4 phase though of porous nature is found to have high thermal and mechanical resistance as well as chemical stability finding application as catalyst support in various chemical reaction [31].

In plasma spray coatings, thermal stress generated during heating and cooling which are typical of aircraft gas-turbine engines are attributed to cracks and voids observed in Fig. 7. The existence of mismatch between thermal expansion coefficients of the oxide scale, coating layers and the substrate are mainly ascribed as the cause of thermal stresses. Generation of such thermal mismatch stresses alternates between compressive and tensile stresses during thermal cycle resulting to crack initiation [32]. The cracks-initiated coalesce to form Kirkendall voids as seen in Fig. 7 with an illustration in Fig. 9 e. The coating layer further undergoes degradation due high susceptibility to cracking and spallation of Al_2O_3 oxide protective scale which is more brittle [26]. The inner layer is thus exposed for further fresh oxidation resulting to outward diffusion of aluminum giving rise to more Kirkendall voids formation which are found to increase with exposure duration as shown schematically in Fig. 9 f. Most of the porosities in the coating are reduced at 750 °C since most of the aluminium are in molten state thus reducing oxygen intake compared to specimens oxidized at 650 °C where most of the aluminum coating layer is in solid state allowing diffusion of more oxygen as observed in Fig. 8. Depletion of aluminum in the coating giving rise to formation of voids as observed during high-temperature exposure is therefore due to; (i) formation of Al_2O_3 oxide, (ii) inward diffusion for the growth of NiAl–intermetallic layers, and (iii) formation of NiAl_2O_4 spinel. As observed in Fig. 2 through Fig. 7, hot-dip coatings have a better cyclic oxidation both in dry and moist air conditions compared to plasma spray coatings and bare specimens. Plasma spray coating failure could be attributed to presence of entrapped oxides and cracks arising during coating process. The hot-dip coating on the other hand performed much better due to excellent adherent of the coating to the substrate with no observable voids, cracks or entrapped oxides.

Acknowledgements

Authors would like to acknowledge financial support of this research by the National Science Council, Taiwan under Grant No. NSC MOST105-2623-E-011-003-D.

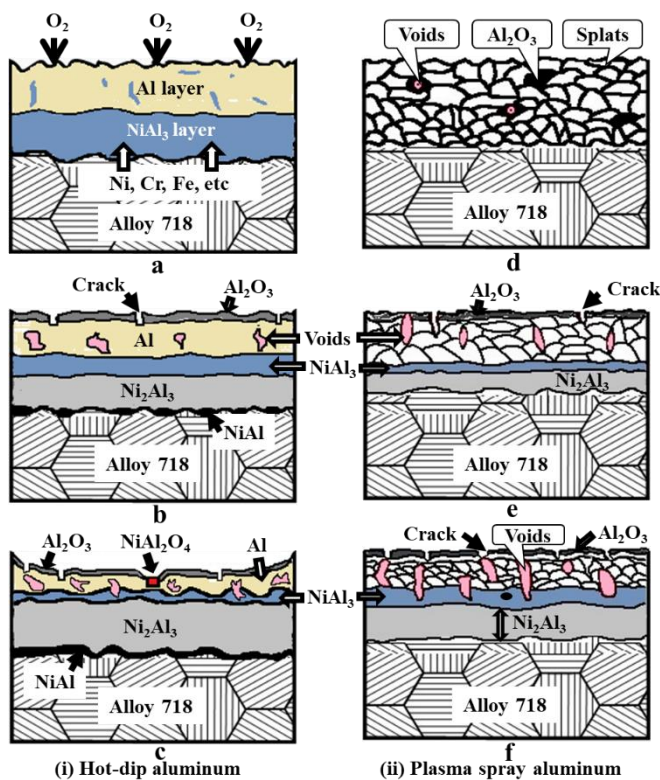


Fig. 9. Schematic illustration of oxidation process on aluminized coated IN 718 in atm. air

5. CONCLUSIONS

Oxidation behavior and mechanisms of inconel 718 coated with aluminum alloy by hot-dip and plasma spray processes was conducted in dry and moist air conditions at different temperatures with exposure time of up to 90 hrs to ascertain their performance. The findings of this study can be summarized as follows:

The hot-dip coatings greatly improved oxidation resistance of the alloy with lowest mass change compared to plasma spray and bare material.

The surface oxide layer formed on hot-dip coatings in dry air consists mainly of Al_2O_3 above the intermetallic aluminide layers of NiAl_3 and Ni_2Al_3 whose thickness increased with duration of cyclic oxidation. However, voids in the aluminum layer increased at each thermal cycle causing depletion of aluminum in the coating with the formation of a porous NiAl_2O_4 spinel.

Moist air caused oxide scale formed in both types of aluminum coatings to crack after five cycles with extensive blistering and spallation. This could be attributed to hydrogen produced by reaction of water vapour with Al or Ni to dissolve in the alloy but released on cooling causing the oxide to blister or spall.

Aluminum coatings are more porous with profound internal voids in moist air. However, water vapour did not appear to cause large effects on hot-dip coating as compared to plasma spray coating.

Thus, it was concluded that hot-dip coating has a better oxidation resistance to improve performance of IN 718 at high temperature applications both in dry and moist air conditions compared to plasma spray coating.

REFERENCES

1. Al-hatab, K.A., Al-bukhaiti, M.A., Krupp, U., Kantehm, M. Cyclic Oxidation Behavior of IN 718 Superalloy in Air at High Temperatures *Oxidation of Metals* 75 (3–4) 2011: pp. 209–228. <https://doi.org/10.1007/s11085-010-9230-6>
2. Zhang, Y.N., Cao, X., Wanjara, P., Medraj, M. Oxide Films in Laser Additive Manufactured Inconel 718 *Acta Materialia* 61 (17) 2013: pp. 6562–6576. <https://doi.org/10.1016/j.actamat.2013.07.039>
3. Mudgal, D., Singh, S., Prakash, S. Cyclic Hot Corrosion Behavior of Superni 718, Superni 600, and Superco 605 in Sulfate and Chloride Containing Environment at 900 °C *Metallography, Microstructure, and Analysis* 4 (1) 2015: pp. 13–25. <https://doi.org/10.1007/s13632-014-0182-0>
4. Mannava, V., Rao, A.S., Paulose, N., Kamaraj, M., Kottada, R.S. Hot Corrosion Studies on Ni-Base Superalloy at 650 °C Under Marine-Like Environment Conditions Using Three Salt Mixture ($\text{Na}_2\text{SO}_4 + \text{NaCl} + \text{NaVO}_3$) *Corrosion Science* 105 2016: pp. 109–119. <https://doi.org/10.1016/j.corsci.2016.01.008>
5. Davis, J.R. ASM Specialty Handbook, Nickel, Cobalt and Their Alloys. 2000, ASM International. pp. 1–186.
6. Chaturvedi, M.C., Han, Y.F. Strengthening Mechanisms in Inconel 718 Superalloy *Metal Science* 17 (3) 1983: pp. 145–149. <https://doi.org/10.1179/030634583790421032>
7. Sundararaman, M., Mukhopadhyay, P., Banerjee, S., Some Aspects of the Precipitation of Metastable Intermetallic Phases in INCONEL 718 *Metallurgical Transactions A* 23 (7) 1992: pp. 2015–2028. <https://doi.org/10.1007/bf02647549>
8. Cozar, R., Pineau, A. Morphology of γ' and γ'' Precipitates and Thermal Stability of Inconel 718 Type Alloys *Metallurgical Transactions* 4 (1) 1973: pp. 47–59. <https://doi.org/10.1007/bf02649604>
9. Jianhong, H., Fukuyama, S., Yokogawa, K. γ'' Precipitate in Inconel 718 *Journal of Material Science Technology* 10(4) 1994: pp. 293–303.
10. Bi, Z.N., Dong, J.X., Zhang, M.C., Zheng, L., Xie, X.S. Mechanism of α -Cr Precipitation and Crystallographic Relationships Between α -Cr and δ Phases in Inconel 718 Alloy After Long-Time Thermal Exposure *International Journal of Minerals, Metallurgy, and Materials* 17 (3) 2010: pp. 312–317. <https://doi.org/10.1007/s12613-010-0310-z>
11. Mahobia, G.S., Paulose, N., Singh, V. Hot Corrosion Behavior of Superalloy IN718 at 550 and 650 °C *Journal of Materials Engineering and Performance* 22 (8) 2013: pp. 2418–2435. <https://doi.org/10.1007/s11665-013-0532-0>
12. Saladi, S., Menghani, J., Prakash, S. Hot Corrosion Behaviour of Detonation-Gun Sprayed Cr_3C_2 -NiCr Coating on Inconel-718 in Molten Salt Environment at 900 °C *T Indian I Metals* 67 (5) 2014: pp. 623–627. <https://doi.org/10.1007/s12666-014-0383-x>
13. Slama, C., Servant, C., Cizeron, G., Aging of the Inconel 718 Alloy Between 500 and 750 °C *Journal of Materials Research* 12 (09) 2011: pp. 2298–2316. <https://doi.org/10.1557/jmr.1997.0306>
14. Zurek, J., Young, D.J., Essuman, E., Hänsel, M., Penkalla, H.J., Niewolak, L., Quadackers, W.J. Growth and Adherence of Chromia Based Surface Scales on Ni-Base

- Alloys in High- and Low-pO₂ Gases *Materials Science and Engineering: A* 477 (1–2) 2008: pp. 259–270.
<https://doi.org/10.1016/j.msea.2007.05.035>
15. **Wang, C.J., Chen, S.M.** Microstructure and Cyclic Oxidation Behavior of Hot Dip Aluminized Coating on Ni-Base Superalloy Inconel 718 *Surface & Coatings Technology* 201 (7) 2006: pp. 3862–3866.
<https://doi.org/10.1016/j.surfcoat.2006.07.242>
 16. **Chen, J.H., Little, J.A.** Degradation of the Platinum Aluminide Coating on CMSX4 at 1100 °C *Surface & Coatings Technology* 92 (1–2) 1997: pp. 69–77.
[https://doi.org/10.1016/S0257-8972\(96\)03117-9](https://doi.org/10.1016/S0257-8972(96)03117-9)
 17. **Visuttipitukul, P., Limvanutpong, N., Wangyao, P.** Aluminizing of Nickel-Based Superalloys Grade IN 738 by Powder Liquid Coating *Materials Transactions* 51 (5) 2010: pp. 982–987.
<https://doi.org/10.2320/matertrans.M2009382>
 18. **Zagula-Yavorska, M., Kubiak, K., Sieniawski, J.** Oxidation Behaviour of Palladium Modified Aluminide Coatings Deposited by CVD Method on Nickel-Based Superalloys Under Air Atmosphere *Journal of Achievements in Materials and Manufacturing Engineering* 55 (2) 2012: pp. 848–854.
 19. **Cheng, W.J., Wang, C.J.** Effect of Chromium on the Formation of Intermetallic phases in Hot-dipped Aluminide Cr-Mo Steels *Applied Surface Science* 277 2013: pp. 139–145.
<https://doi.org/10.1016/j.apsusc.2013.04.015>
 20. **Zielinska, M., Sieniawski, J., Yavorska, M., Motyka, M.** Influence of Chemical Composition of Nickel Based Superalloy on the Formation of Aluminide Coatings *Archives of Metallurgy and Materials* 56 (1) 2011: pp. 193–197.
<https://doi.org/10.2478/v10172-011-0023-y>
 21. **ASM-International,** ASM Handbook: Volume 3: Alloy Phase Diagrams. 1992, Materials Park, Ohio: ASM International.
 22. **Jiang, S.Y., Li, S.C.** Formation Mechanism and Prediction of New Phases in Binary Metallic Liquid/Solid Interface *Rare Metals* 30 (S1) 2011: pp. 486–491.
<https://doi.org/10.1007/s12598-011-0330-5>
 23. **Birks, N., Meter, G.H., Pettit, F.S.** Introduction to the High-Temperature Oxidation of Metals. 2006, Cambridge University Press: United States of America. pp. 352.
 24. **Chevalier, S., Juzon, P., Przybylski, K., Larpin, J.P.** Water Vapor Effect on High-Temperature Oxidation Behavior of Fe₃Al Intermetallics *Science and Technology of Advanced Materials* 10 (4) 2009: pp. 1–7.
<https://doi.org/10.1088/1468-6996/10/4/045006>
 25. **Rouaix-Vande Put, A., Unocic, K.A., Brady, M.P., Pint, B. A.,** Performance of Chromia- and Alumina-Forming Fe- and Ni-Base Alloys Exposed to Metal Dusting Environments: The Effect of Water Vapor and Temperature *Corrosion Science* 92 2015: pp. 58–68.
<https://doi.org/10.1016/j.corsci.2014.11.022>
 26. **Stott, F.H.** The Protective Action of Oxide Scales in Gaseous Environments at High Temperature *Reports on Progress in Physics* 50 (7) 1987: pp. 861–913.
<https://doi.org/10.1088/0034-4885/50/7/002>
 27. **Wang, C.J., Badaruddin, M.** The Dependence of High Temperature Resistance of Aluminized Steel Exposed to Water-Vapour Oxidation *Surface and Coatings Technology* 205 (5) 2010: pp. 1200–1205.
<https://doi.org/10.1016/j.surfcoat.2010.08.153>
 28. **Yan, K., Guo, H., Gong, S.** High-Temperature Oxidation Behavior of β-NiAl With Various Reactive Element Dopants in Dry and Humid Atmospheres *Corrosion Science* 83 2014: pp. 335–342.
<https://doi.org/10.1016/j.corsci.2014.02.033>
 29. **Goward, G.W., Boone, D.H.** Mechanisms of Formation of Diffusion Aluminide Coatings on Nickel-Base Superalloys *Oxidation of Metals* 3 (5) 1971: pp. 475–495.
<https://doi.org/10.1007/bf00604047>
 30. **Zygmuntowicz, J., Wicińska, P., Miazga, A., Konopka, K.** Characterization of Composites Containing NiAl₂O₄ Spinel Phase from Al₂O₃/NiO and Al₂O₃/Ni Systems *Journal of Thermal Analysis and Calorimetry* 125 (3) 2016: pp. 1079–1086.
<https://doi.org/10.1007/s10973-016-5357-2>
 31. **Anchieta, C.G., Tochetto, L., Madalosso, H.B., Sulkowski, R.D., Serpa, C., Mazutti, M.A., de Almeida, A.R.F., Gündel, A., Foletto, E.L.** Effect of Thermal Treatment on the Synthesis of NiAl₂O₄ Spinel Oxide Using Chitosan as Precursor *Cerâmica* 61 (360) 2015: pp. 477–481.
<https://doi.org/10.1590/0366-69132015613601925>
 32. **Thouless, M.D.** Cracking and Delamination of Coatings *Journal of Vacuum Science & Technology A: Vacuum, Surfaces, and Films* 9 (4) 1991: pp. 2510–2515.
<https://doi.org/10.1116/1.577265>